

# Improvement of Accuracy based on Multi-Sample and Multi-Sensor in the Gait-based Authentication using Trouser Front-Pocket Sensors

Shinsuke Konno<sup>\*</sup>, Yoshitaka Nakamura<sup>\*\*</sup>, Yoh Shiraishi<sup>\*\*</sup>, and Osamu Takahashi<sup>\*\*</sup>

<sup>\*</sup> National Institute of Technology, Hakodate Collage, Japan

<sup>\*\*</sup> School of Systems Information Science, Future University Hakodate, Japan

skonno@hakodate-ct.ac.jp

{y-nakamr, siraisi, osamu}@fun.ac.jp

**Abstract** - Nowadays, smartphones are equipped with various personal authentication functions to prevent imposters from misusing. However, low utilization rate of personal authentication functions caused by the inconvenient operations becomes the problem. To reduce the inconvenience, authentication methods based on behavior characteristics have been studied. Gait-based authentication is one of them. This authentication method automatically identifies individuals based on walking motions measured by smartphone sensors. The purpose of this study is to find the appropriate methods in each authentication process and to improve the authentication accuracy. For these purpose, we tested the various distance calculation methods, and four fusion algorithms. As this result, we found the appropriate methods in each process. Furthermore, by applying these appropriate methods to the authentication system, the authentication accuracy was significantly improved in comparison with previous studies.

**Keywords:** gait-based authentication, acceleration sensor, gyro sensor, dynamic time warping, score level fusion

## 1 INTRODUCTION

The use of portable terminals such as smartphones has increased in recent years and can be expected to increase in the future. Though initially used mainly for telephone calls, text messages, and browsing, nowadays such devices also serve many other important functions, such as making payments and storing private and business information. Accordingly, smartphones and other portable terminals have become loaded with various functions intended to prevent misuse by imposters. One of these is personal authentication, for which there are many methods, such as personal identification numbers (PINs) and passwords. Recently, methods such as pattern locks, which are more difficult for an imposter to break, has been incorporated into the devices. Furthermore, terminals with biometric identification using fingerprints or face images have been developed. As these examples illustrate, developers are making serious efforts to prevent improper use of these devices. On the other hand, there are reports and news items showing that approximately 50% of users do not use personal authentication on their devices, perhaps because they feel that the authentication methods are too difficult to use. Previous studies proposed easier authentication methods by extracting individual features of device operation, such as swinging the terminal or tapping on the display. However these methods require con-

scious action, so they cannot perform authentication in the background.

On the other hand, it is conceivable that individual authentication might be established through daily repeated activities. With such a method, users can unlock their terminal without conscious authentication operations. Gait-based authentication is one example of an unconscious method of this type. The Ministry of Health, Labour and Welfare reported that Japanese adult men walk an average of 7,099 steps in a day. Furthermore, we think that walking is performed in various situations. If gait-based authentication was established, the inconvenience users feel in individual authentication would be reduced. There are many scenes when we want to unlock our smartphones quickly and automatically in daily life. Examples are automatic-ticket gate and payment with IC card of smartphone at the cash desk. Furthermore, this authentication system can identify the owner without conscious operation repeatedly. Therefore, this authentication system can use as the theft detecting system. This authentication system can develop with the simple sensors. So, there is a research which proposed that this authentication system was built into smart key system for cars.

We work with multi-modal authentication to improve authentication performance by combining multiple methods in individual authentication [1].

Fernand et al. [2] combined faces and fingerprints to improve accuracy. Zhou et al. [3] combined features of side face and gait using principal component analysis to identify people, and many other researchers have also attempted to improve accuracy using biometric authentication.

However, wearing multiple sensors on various body parts sacrifices convenience, the advantage of gait authentication. For this reason, we adopt a method that combines multiple sensor methods measuring the same body parts using multiple sensors, and a multi-sample method that measures a modality several times to improve performance. It is possible to equip a terminal with multiple sensors, enabling us to authenticate using multiple sensors without imposing a burden on users.

In this study, we use two sensors (a three-axis acceleration sensor and a three-axis gyro sensor) to measure human walking motion. We show that the proposed method, which combines distance information recorded by these two sensors, improves authentication accuracy in comparison with previous studies.

Table 1: Summary of gait-based authentication work.

work	position	Sensor
Mäntyjärvi et al. [4]	belt	acceleration
Gafurov et al. [5]	hip	acceleration
Gafurov et al. [6]	ankle	acceleration
Gafurov et al. [7]	trouser pocket	acceleration
Gracian et al. [8]	belt	acceleration
Derawi et al. [9]	belt	acceleration
Soumik et al. [10]	eight-joints	rotation angle

## 2 RELATED WORK

There has been related work on authentication using wearable sensors for walking motions. The most common approach is to use acceleration sensors fixed at the user's waist. We explain the details of that work in this section.

### 2.1 Position of Sensors

Table 1 summarizes the related work. These studies explored features and authentication methods primarily to improve performance. However, they did not investigate which sensor positions would be acceptable for daily use. Those studies measured mainly using devices attached on the belt on the middle or side of the waist, and authenticated subjects based on the acceleration signals. This requires using a smartphone case such as a holster for attaching the terminal to the waist. Users might find this unacceptable, because gait authentication then requires them to have the container with them. Consequently, we decided that the trouser front-pocket might be acceptable to users, because they can then have the terminal without using special tools, and we investigated performance improvement in this position. The study in [7] examined this position. This study aims to improve authentication performance in comparison to that previous study.

### 2.2 Fusion of Multiple Sensors

Many acceleration-based approaches to gait-based authentication have been explored.

Mäntyjärvi et al. [4] proposed three authentication methods: fast Fourier transform, correlation, and statistical features.

Gafurov et al. [5]-[7] studied methods based on acceleration, and made measurements by using acceleration sensors on various parts of subject's bodies. They used a template signal and multiple time-normalized signals, with the acceleration sensor placed in the trouser front pocket [7].

Gracian et al. [8] devised the feature of gait acceleration for user authentication.

Derawi et al. [9] proposed a multi-sampling method that authenticated using multiple signals from both templates and inputs. Their method calculated distances of all combinations of templates and inputs with dynamic time warping (DTW).

Soumik et al. [10] measured walking motions with eight angle sensors attached on various joints.

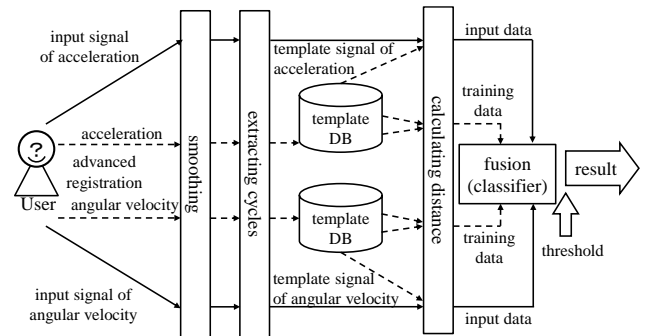


Figure 1: Overview of the proposed system.

To the best of our knowledge, there are no studies on the fusion of multiple sensors placed in a trouser front pocket. In this study, to improve authentication accuracy, we propose a method of fused distances based on acceleration and angular velocity placed in a trouser front pocket.

## 3 PROPOSED METHOD

### 3.1 Overview

Figure 1 shows an overview of the proposed authentication method. This method authenticates users based on distances among input and template signals in the time domain. Template signals are registered in the database in advance.

Gait signals show similar waveforms repeatedly for each subject. We expect that when genuine, the distance between input and template signals is small, and when from an imposter, the distance is greater. Consequently, we considered that it is possible to generate a common classifier among all users for authentication. When we fuse distances calculated from multiple sensors, we use a common classifier in all subjects.

When the system employed multi-sample method, users need to walk long distances for multiple input signals to be used for authentication. Therefore, we consider that multi-sample authentication must calculate the distance between an input signal and the multiple template signals registered.

### 3.2 Gait Recognition and Quasi-Periodic Signal Extraction

We attached a sensor unit whose x-, y-, and z-axis detected vertical, sideway, and forward-backward acceleration, respectively, in standing posture. The direction of each axis is shown in Fig. 2. Each signal of a gyro sensor detects an angular velocity whose rotary axis is identical to each axis of an acceleration sensor. Each subject wore a sensor unit attached to a belt with hook and loop fastener. This unit was placed on the front of the left femur area.

Examples of three-axis acceleration and three-axis angular velocity are shown in Fig. 3 and 4. During walking, the acceleration and gyro sensors measured similar waveforms repeatedly. These signals are quasi-periodic signals with no equalization of cycles and amplitudes. The length of a gait cycle is two steps. The gait cycle consists of four periods, double limb support (in left stance phase), single limb support (in right swing phase), double limb support (in right

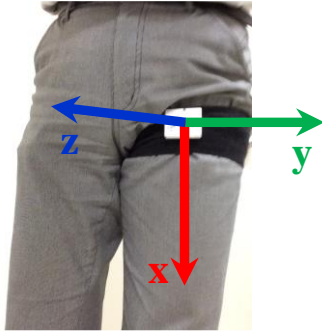


Figure 2: Directions of three axes.

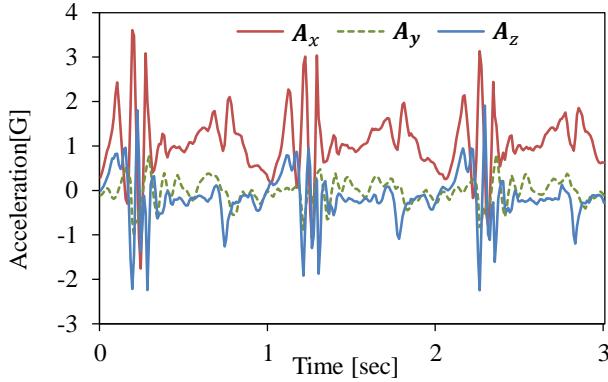


Figure 3: Example of gait signals from three-axis acceleration sensor.

stance phase) and single limb support (in left swing phase). We walk forward by repeating the four periods. If we change the start period of the signal extraction for each user to obtain the input signals and the template signals whose lengths are two steps, we extract the signals with different order of periods for each user. As a result, we obtain their signals with different waveform among users and may achieve good performance seemingly in authentication. To prevent influence on authentication accuracy by different waveform for each user, we decided to extract their quasi-periodic signals with the same order of the gait periods to all users. For this reason, we conducted a preliminary experiment to investigate the relation between walking motion and six-axis signals. To measure the time from a left heel touching ground to its rising from the ground, two force sensors synchronized with the sensor unit were attached to their left toe and heel. Examples of the acceleration along the x-axis and the signal of the force sensor are shown in Fig. 5. The graph shows that the time when the acceleration becomes a local maximum is approximately equal to the time when the value of the force sensor under the left heel begins to increase. This result indicates that the time when the acceleration becomes a local maximum coincides with the time when the left heel lands on the ground. Hence, we extract these quasi-periodic signals of the same walking motion period in the different subjects using the following method.

### 3.2.1 Walking Detection

In this study, we use a threshold in vertical acceleration to detect walking start time based on previous research [7].

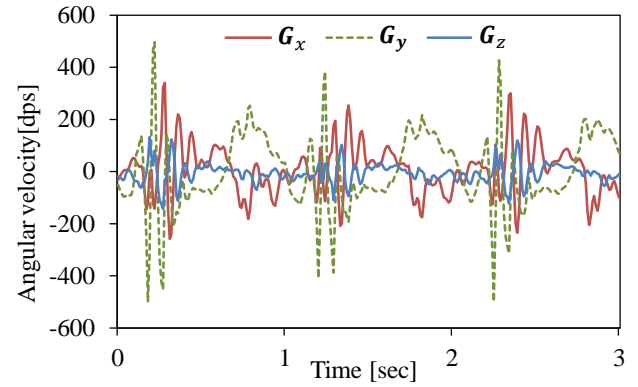


Figure 4: Example of gait signals from three-axis angular gyro sensor.

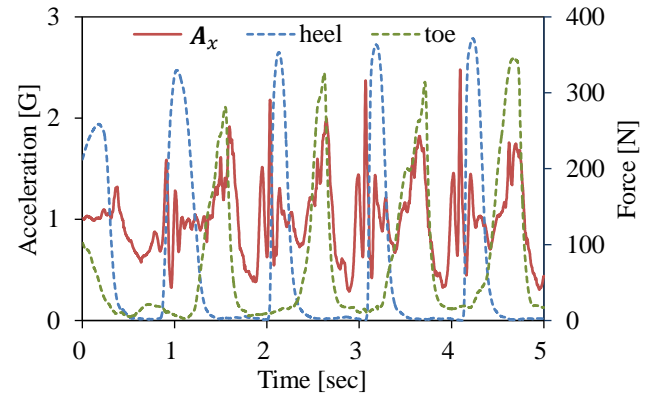


Figure 5: Example of the vertical acceleration signal and force signal.

Before beginning, all signals were smoothed using a Savitzky-Golay filter [11]. We look for the time  $t_s$  when the acceleration is greater than 1.2 G from the start of this quasi-periodic signal extraction method.

### 3.2.2 Quasi-Periodic Signal Extraction

After detection, we extract quasi-periodic signals measuring the period between left-heel landings on the ground. The extraction process with x-axis acceleration  $A_x$  is as follows:

- 1) We search for the maximum time  $T_0$  within two seconds after walking detection  $t_s$ . We selected  $T_0$  as the start time of cycle  $C_0$ . For reference, the process of detecting  $T_0$  is shown in Fig. 6.
- 2) To find the end time of  $C_0$ , we search for all times of local maxima  $\mathbf{t}_1 = \{t_{11}, t_{12}, t_{13} \dots\}$  from 0.7 to 1.3 s after  $T_0$  from  $A_x$ .
- 3) We extract subsets  $\mathbf{s}_0$  that are 0.6 s of the signal.  $T_0$  is the middle time of subset  $\mathbf{s}_0$ . In the same way, each element in  $\mathbf{t}_1$  is the middle time of subsets  $\mathbf{S}_1 = \{\mathbf{s}_{11}, \mathbf{s}_{12}, \mathbf{s}_{13} \dots\}$ , whose subsets are extracted as 0.6 s signals. For example,  $\mathbf{s}_{11}$  are 0.6s of extracted signal whose middle time is  $t_{11}$ . We calculate values  $\mathbf{N}_1 = \{N_{11}, N_{12}, N_{13} \dots\}$  of the normalized cross correlation (NCC) among  $\mathbf{s}_0$  and each element in  $\mathbf{S}_1$ . We take the middle time of  $\max(\mathbf{N}_1)$  as the start time  $T_1$  of the next cycle  $C_1$ . Figure 7 shows an example of detecting  $T_1$ . As a result of the calculations using NCC, we take  $t_{13}$  as  $T_1$ .

Through this processing, we obtain one cycle  $C_0$  by extracting  $A_x$  from  $T_0$  to  $T_1$ .

- 4) Next, we search for all times of local maxima  $t_2 = \{t_{21}, t_{22}, t_{23} \dots\}$  from 0.7 to 1.3 s after  $T_1$ . We extract subsets of signal  $S_2 = \{s_{21}, s_{22}, s_{23} \dots\}$  from  $T_1$  to each  $t_2$ . We calculate distances  $d_2 = \{d_{21}, d_{22}, d_{23} \dots\}$  between  $C_0$  and each  $S_2$  using DTW. To eliminate the effect of differences in signal length, we divided each distance by the total length of  $C_0$  and each  $S_2$ . We take the time  $t_{22}$  of minimum distance as the start time  $T_2$  of the next cycle  $C_2$ .
- 5) After the time  $T_n$  of minimum distance is calculated using DTW among  $C_{n-1}$  and  $S_n$ , we begin searching for the next start time  $T_{n+1}$  by repeating step 4).
- 6) When forward searching is completed, we repeat the process by searching backward at  $T_0$ .
- 7) The end time of an extracted cycle duplicates the start time of the next cycle. Hence, we eliminated amplitude of end time from each extracted cycle.
- 8) When we observed the extracted signals, we found that those near the signals of starting to walk had a large distortion as compared with other signals. Based on the result of analysis, the variance of each signal with a large distortion is smaller than the variance of other signals. Hence, we searched for the first distorted signals whose variance was greater than the threshold 0.09. We assumed that the signals used for authentication were signals subsequent to it. Examples of the variance from extracted signals are shown in Fig. 9. In this x-axis acceleration, we took the signals to be used for authentication as the cycles after  $C_0$ . We recorded the starting times of extracted cycles, and extracted signals for the other two-axis acceleration and three-axis angular velocity using the same starting time.

The x-axis signals extracted by this method are shown in Fig. 10 and 11. Figure 10 shows two quasi-periodic signals extracted from the same subject. In Fig. 11, the solid and dotted lines indicate extracted quasi-periodic signals from different subjects.

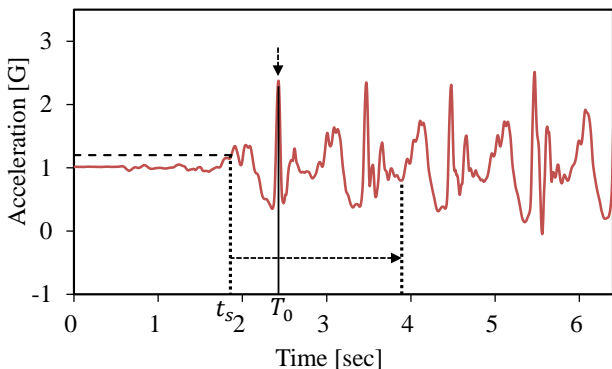


Figure 6: Example of detection of start time  $t_0$  of cycle  $C_0$ .

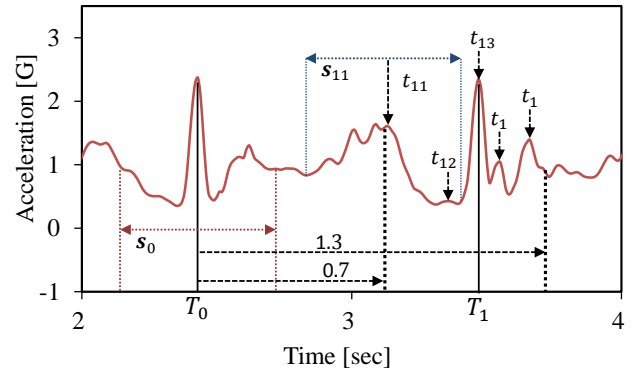


Figure 7: Example of detection of start time  $t_1$  of cycle  $C_1$ . Lower-arrows indicate the local maxima between 0.7 and 1.3 s after  $T_0$ .

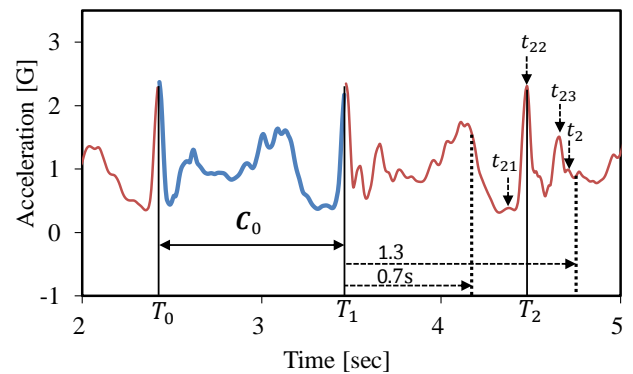


Figure 8: Example of extracted cycle  $C_0$  and local maximum  $t_2$ .

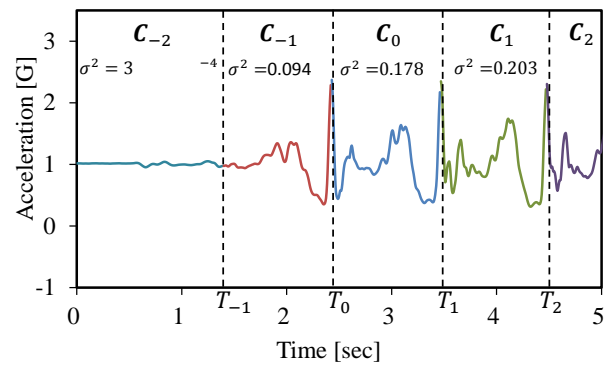


Figure 9: Example of extracted cycles and their variances.

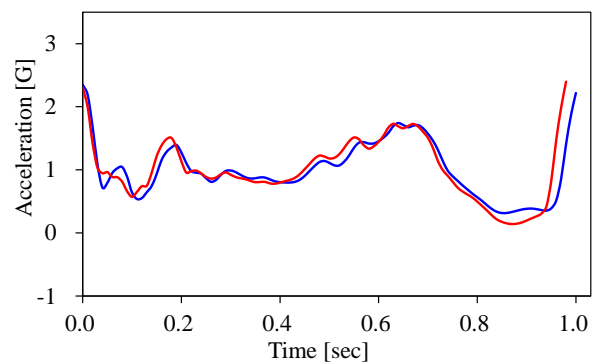


Figure 10: Extracted signals from same subject.

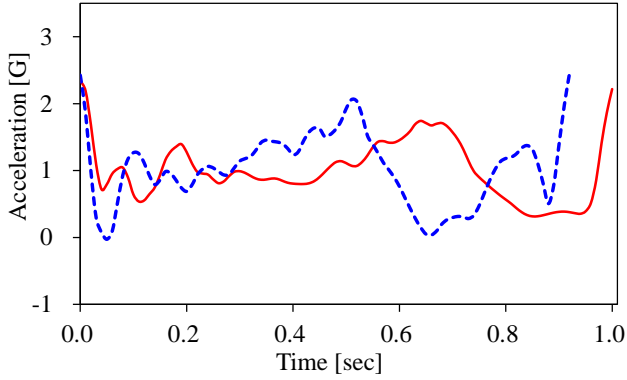


Figure 11: Extracted signals from two subjects.

### 3.3 Distance Calculation Methods

To find the better method, we tested DTW and linear interpolation which equalize the length of two signals. These are frequently used for calculating dissimilarity as a distance between time series data. Let  $\mathbf{X} = \{x(i)|i = 1, 2, \dots, m\}$ ,  $\mathbf{Y} = \{y(j)|j = 1, 2, \dots, n\}$  be time series data. The distance by DTW between  $\mathbf{X}$  and  $\mathbf{Y}$  is defined as

$$D_{DTW}(\mathbf{X}, \mathbf{Y}) = f(m, n)$$

$$f(i, j) = \min \begin{cases} f(i-1, j-1) + \text{dist}(x(i), y(j)) \\ f(i, j-1) + \text{dist}(x(i), y(j)) + GP \\ f(i-1, j) + \text{dist}(x(i), y(j)) + GP \end{cases}$$

$$f(0, 0) = 0, \quad f(1, 0) = f(0, 1) = \infty$$

where  $D_{DTW}(\mathbf{X}, \mathbf{Y})$  is the distance calculated using DTW,  $m$  and  $n$  are the number of lengths in signals  $\mathbf{X}$  and  $\mathbf{Y}$ , and  $GP$  is a gap penalty in the case of non-linear extension. We adopted the different distance calculation method for each sensor. The distance calculation function is substituted into  $\text{dist}(x(i), y(j))$ . Next, to adapt the differences of signal length by differences of walking speed, we normalized the distance by dividing the total length of the two signals. The normalized distance  $D(\mathbf{X}, \mathbf{Y})$  is calculated as

$$D(\mathbf{X}, \mathbf{Y}) = \frac{D_{DTW}(\mathbf{X}, \mathbf{Y})}{m + n}$$

Similarly, in the case of linear interpolation, the length of  $\bar{\mathbf{X}}$  and  $\bar{\mathbf{Y}}$  was equalized to the longer length between  $\mathbf{X}$  and  $\mathbf{Y}$  using linear interpolation to  $\mathbf{X}$  and  $\mathbf{Y}$ . The normalized distance  $D(\mathbf{X}, \mathbf{Y})$  is calculated as

$$D(\mathbf{X}, \mathbf{Y}) = \begin{cases} \frac{D_{LI}(\bar{\mathbf{X}}, \bar{\mathbf{Y}})}{2m} & (m \geq n) \\ \frac{D_{LI}(\bar{\mathbf{X}}, \bar{\mathbf{Y}})}{2n} & (m < n) \end{cases}$$

where  $D_{LI}(\bar{\mathbf{X}}, \bar{\mathbf{Y}})$  is the distance between  $\bar{\mathbf{X}}$  and  $\bar{\mathbf{Y}}$ .

In the multi-sample case, we used the median as the distance. Let  $\mathbf{Y} = \{\mathbf{Y}_1, \mathbf{Y}_2, \dots, \mathbf{Y}_k, \dots, \mathbf{Y}_p\}$  be multiple template signals. This distance was calculated as

$$D(\mathbf{X}, \mathbf{Y}) = \text{median}_{k=1, 2, \dots, p}(D(\mathbf{X}, \mathbf{Y}_k))$$

where  $D(\mathbf{X}, \mathbf{Y}_k)$  is the normalized distance between an input signal and  $k$ -th template signals of multiple template signals.

#### 3.3.1 Angular Velocity Distance

It is known that angular velocity does not depend on distance from the center of rotation. We calculate the absolute distance between the input signal and template signals. Even if signals of the same subject are selected, they do not correspond to the amplitude value from a difference in walking speed. To reduce differences between signals of the same subject, we normalized the signals by dividing the amplitude of each time by specific values. We adopted the method of normalization that divides amplitude of signal by the root mean square (RMS). The reason for using RMS for normalization is that it provided the best accuracy among some normalized methods in a preliminary experiment.

Let  $\mathbf{g}_q = (g_q(1), g_q(2), \dots, g_q(i), \dots, g_q(m))$  be the  $q$ -axis input angular velocity signal, and let  $\mathbf{g}'_{qk} = (g'_{qk}(1), g'_{qk}(2), \dots, g'_{qk}(j), \dots, g'_{qk}(n))$  be the  $k$ -th template in  $q$ -axis angular velocity signal. We tested three distance calculation methods. They were Euclidean distance, Manhattan distance (absolute distance), and the distance based on correlation (denoted as Crr distance).

In the case of linear interpolation, Manhattan distance between a  $q$ -axis input angular velocity signal and a  $k$ -th template in  $q$ -axis angular velocity signal was calculated as

$$D_{LI}(\bar{\mathbf{g}}_q, \bar{\mathbf{g}}'_{qk}) = \sum_l |\bar{g}_q(l) - \bar{g}'_{qk}(l)|$$

Euclidean distance was calculated as

$$D_{LI}(\bar{\mathbf{g}}_q, \bar{\mathbf{g}}'_{qk}) = \sqrt{\sum_l (\bar{g}_q(l) - \bar{g}'_{qk}(l))^2}$$

Crr distance was not divided by the total length of two signals, because signal length is not affected on the correlation value. Therefore, in the case of Crr distance calculation,  $D(\mathbf{g}_q, \mathbf{g}'_{qk})$  was calculated as

$$D(\mathbf{g}_q, \mathbf{g}'_{qk}) = 1 - NCC(\bar{\mathbf{g}}_q, \bar{\mathbf{g}}'_{qk})$$

where  $NCC()$  is the normalized cross correlation between  $\bar{\mathbf{g}}_q$  and  $\bar{\mathbf{g}}'_{qk}$ .

In the case of distance calculation using DTW, Euclidean distance calculation function  $\text{dist}(g_q(i), g'_{qk}(j))$  was calculated as

$$\text{dist}(g_q(i), g'_{qk}(j)) = (g_q(i) - g'_{qk}(j))^2$$

Finally, we calculated Euclidean distance with DTW as

$$D_{DTW}(\mathbf{g}_q, \mathbf{g}'_{qk}) = \sqrt{f(m, n)}$$

Manhattan distance calculation function was calculated as

$$\text{dist}(\mathbf{g}_q(i), \mathbf{g}'_{qk}(j)) = |\mathbf{g}_q(i) - \mathbf{g}'_{qk}(j)|$$

Crr distance cannot be calculated using DTW. Thus, in the case of DTW, we calculated only two types of distance.

### 3.3.2 Acceleration Distance

It is known that acceleration depends on the distance from the center of rotation in the circular motion. If different amplitude normalizations are applied to each axis acceleration, they are compressed at different ratios at the same time. As a result, when the normalized accelerations of the three axes at the same time were combined as a vector, the direction of the vector was changed before normalization. This problem was caused by comparing it with the values of acceleration. Hence, we compared it with the direction of three-axis acceleration between the input and the template acceleration signals [12]. Let  $\mathbf{a}(i)$  be the  $i^{\text{th}}$  input acceleration vector of an input signal, and let  $\mathbf{a}'_k(j)$  be the  $j^{\text{th}}$  template acceleration vector of a  $k$  template signal.

$$\begin{aligned} \mathbf{a}(i) &= (a_x(i), a_y(i), a_z(i)) \\ \mathbf{a}'_k(j) &= (a'_{xk}(j), a'_{yk}(j), a'_{zk}(j)) \end{aligned}$$

where  $a_q(i)$  is the  $q$ -axis  $i^{\text{th}}$  amplitude of input acceleration signal, and  $a'_{qk}(j)$  is the  $q$ -axis  $j^{\text{th}}$  amplitude of  $k$ -th template acceleration signal. The difference of direction between the  $i^{\text{th}}$  input acceleration vector and  $j^{\text{th}}$   $k$ -th template acceleration vector was calculated as

$$\text{dist}(\mathbf{a}(i), \mathbf{a}'_k(j)) = \arccos \frac{\langle \mathbf{a}(i), \mathbf{a}'_k(j) \rangle}{\|\mathbf{a}(i)\| \|\mathbf{a}'_k(j)\|}$$

The distance based on difference of direction is calculated using DTW by substituting this function into  $\text{dist}()$ .

To compare this three-axis composite method with others, authentication accuracy of each axis acceleration was calculated using the same normalization and distance calculation method for angular velocity.

### 3.4 Distance Fusion

In biometrics authentication, score fusions were attempted using various methods [1], [13].

To eliminate subject dependency, we subtracted the average distance from the distance before fusion. This average distance was calculated between a subject's template signal  $\mathbf{Y}$  and the same subject's recorded data  $\boldsymbol{\gamma}$  except his or her template signal  $\mathbf{Y}$ . This averaged distance was calculated with the all template signals selected in the evaluation. In the case of multi-sampling, the average distance of template signals  $\overline{D}(\boldsymbol{\gamma}, \mathbf{Y})$  is an averaged distance of medians calculated among all combinations of template signals using the same calculation of the median between an input signal and

multiple template signals. This averaged value was calculated as one value for a subject by using the subject's all selected template signals with replacing the template signals from subject's recorded signal. The normalized distance is calculated by subtracting the average distance from the distance calculated by DTW between an input signal and the template signals as

$$D_s(\mathbf{X}, \mathbf{Y}) = D(\mathbf{X}, \mathbf{Y}) - \overline{D}(\boldsymbol{\gamma}, \mathbf{Y})$$

Finally, two types of fused distance  $D_f$  were calculated as

$$D_f = f(D_s(\mathbf{a}, \mathbf{a}'), D_s(\mathbf{g}_x, \mathbf{g}'_x), D_s(\mathbf{g}_y, \mathbf{g}'_y), D_s(\mathbf{g}_z, \mathbf{g}'_z))$$

$$D_f = f(D_s(\mathbf{a}, \mathbf{a}'), D_s(\mathbf{a}_x, \mathbf{a}'_x), D_s(\mathbf{a}_y, \mathbf{a}'_y), D_s(\mathbf{a}_z, \mathbf{a}'_z), D_s(\mathbf{g}_x, \mathbf{g}'_x), D_s(\mathbf{g}_y, \mathbf{g}'_y), D_s(\mathbf{g}_z, \mathbf{g}'_z))$$

where  $f()$  is a function of fusion which combines the distances. In the our previous experiment, we found that the authentication from the four distances (difference of the direction between acceleration vectors and each axis angular velocity signal) outperformed the authentication from six distances (each axis acceleration signal and each axis angular velocity signal). Therefore, the accuracy from six distances was not verified in this study.

We consider four rules for fusing distances as below.

- (1) Addition without weight coefficients (denoted as Sum)
- (2) Support vector machine (SVM) with a linear kernel (denoted as Linear)
- (3) SVM with a radial basis function kernel (denoted as RBF)
- (4) Linear logistic regression (denoted as LLR)

In calculations using SVM, the classifier must learn based on training dataset. In this study, we obtained too many negative instances as compared with positive instances. Such datasets are said to be imbalanced. It is well known that SVM performs poorly in this case. Hence, we applied the synthetic minority over-sampling technique (SMOTE) [14] to adjust the number of these instances. This algorithm adds the instances among instances based on the  $k$ -nearest neighbor algorithm for the small instances.

## 4 EXPERIMENT

### 4.1 Index of Performance

We evaluated accuracy by equal error rate (EER). The EER is obtained from the intersection of the false acceptance rate (FAR) and the false rejection rate (FRR). An example of EER is shown in Fig. 12.

### 4.2 Dataset

Data was collected from 50 subjects, ranging in age from 18 to 21 years old. We instructed the subjects to walk at their normal walking speeds. When the measurement began, the subjects remained stationary for a few seconds. After that, they walked a specified distance once. The measurement course is a flat and straight indoor passageway. The

subjects did not use a clock or metronome to measure their walking speed.

We set the sampling frequency of the sensor unit to 1,000 Hz. To equalize the performance of the smartphone's sensors, we changed the sampling frequency from 1,000 to 100 Hz by thinning out.

We obtained 30 signals of each axis acceleration and 30 signals of each axis angular velocity from every subject.

### 4.3 Experiment for Distance Calculation

Proposed authentication method is combined multiple processes. Verifying the all combinations of all methods of all processes needs too many times. Therefore, we applied step-by-step evaluation to find the appropriate method in each process.

To reveal the most appropriate distance calculation methods for each sensor, the authentication accuracy in uni-sensor uni-sample authentication was calculated by each distance calculation method. Table 2, and 3 show the EERs for uni-sensor uni-sample methods. The distance calculation combinations of DTW and Manhattan distance showed the best performance with each axis signal of two sensors. Therefore, this combination was employed as features of fusion functions.

### 4.4 Experiment for Verification of Fusion Effectiveness

To verify the effectiveness of each proposed method, we evaluate the four combinations. These are uni-sensor uni-sample combination, uni-sensor multi-sample combination, multi-sensor uni-sample combination, and multi-sensor multi-sample combination. Uni-sensor used one axis of a sensor. Multi-sensor calculated a fused score from six axes signals. Uni-sample used one template signal. Multi-sample used six template signals.

#### 4.4.1 Experimental Setting

We divided the signals into five groups and performed five-fold cross-validation. To generate a fusion model, we used four groups as training data, and one group as test data. We calculated the distances between all of the training signals of all subjects. The distances between the same subjects are positive instances, and the distances between different

subjects are treated as negative instances. The overall accuracies were calculated with common thresholds to each classifier in each fusion rule.

Template signals used for calculating distance include six signals, because the number of template signals is equal to the number of template signals of the previous study [7]. The manner of selecting templates from training data was to select six sequential signals from 24 signals. However, when some of the sequential six signals were selected as test data by cross-validation, we selected the signals in sequence from the nearest start time in the training data.

#### 4.4.2 Experimental Result

For comparison purposes, we calculated EERs of uni-sensor uni-sample (one-axis and one template), uni-sensor multi-sample (one-axis and six templates), multi-sensor uni-sample (six-axis fusion and one template), multi-sensor multi-sample (six-axis fusion and six templates), and previous work [7]. The method used in this previous work created an authentication signal from six signals that were normalized for time length. They were calculated as the absolute distance between a template signal and an input signal.

We summarized the EERs in Tables 4, 5, and 6. The minimum EER (the best result) was 1.0%, which was achieved by the proposed multi-sensor multi-sample method from four distances with two SVMs. The best EER from the template generation and the distance calculation method of the previous work [6] to each axis signal for this dataset was 7.8%. Proposed method could outperform the previous study method.

Figures 13, 14, 15, and 16 show the receiver operating characteristics (ROC) curves for uni-sensor acceleration, uni-sensor angular velocity, multi-sensor fusion from four distances, and multi-sensor fusion from seven distances. These graphs show trade-off relations between the FAR and FRR. To compare the performance of each multi-sensor method, we plotted the ROC curves whose methods showed the best EER in the each combination in Fig. 17. From this ROC curve, we can observe that authentication method multi-sensor multi-sample with 4 distances shows the best performance.

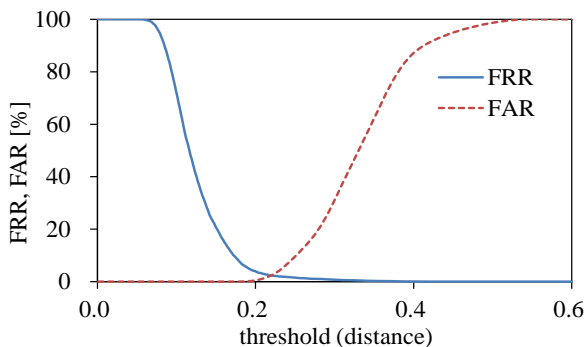


Figure 12: Determining EER.

Table 2: EERs [%] by each distance calculation method with DTW.

	Manhattan distance	Euclidean distance
$a_x$	8.8	10.4
$a_y$	5.3	6.0
$a$	4.6	6.2
$g_x$	6.6	7.0
$g_y$	8.2	9.7
$g$	7.4	8.9

Table 3: EERs [%] by each distance calculation method with linear interpolation.

	Manhattan distance	Euclidean distance	Crr distance
$a_x$	14.0	20.5	19.2
$a_y$	11.2	14.1	7.9
$a$	13.4	18.3	11.6
$g_x$	14.1	15.9	11.2
$g_y$	15.0	18.9	16.3
$g$	15.2	19.1	9.5

Table 4: Uni-sensor EERs [%].

	Uni-sensor uni-sample authentication	Uni-sensor multi-sample authentication
$a_x$	8.8	4.5
$a_y$	5.3	2.2
$a$	4.6	2.2
$g_x$	6.6	2.4
$g_y$	8.2	3.1
$g$	7.4	3.0

Table 5: Multi-sensor EERs [%] fused four distances.

	Multi-sensor uni-sample authentication	Multi-sensor multi-sample authentication
Sum	1.7	1.2
Linear	1.5	1.0
RBF	1.4	1.0
LLR	1.5	1.1

Table 6: Multi-sensor EERs [%] fused seven distances.

	Multi-sensor uni-sample authentication	Multi-sensor multi-sample authentication
Sum	1.5	1.1
Linear	1.4	1.2
RBF	1.2	1.1
LLR	1.5	1.3

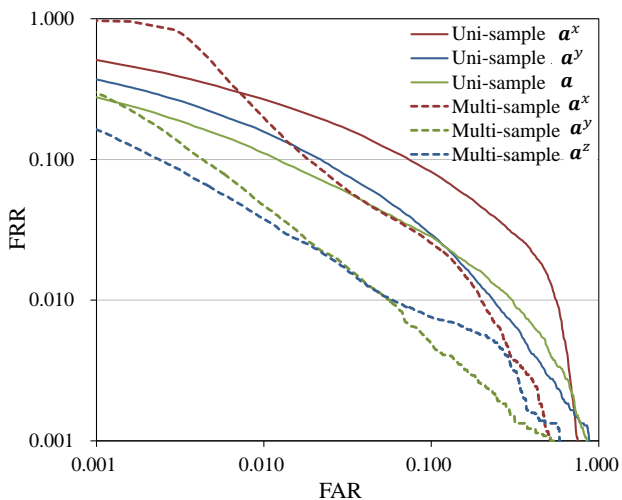


Figure 13: ROC curves of uni-sensor method for three-axis acceleration.

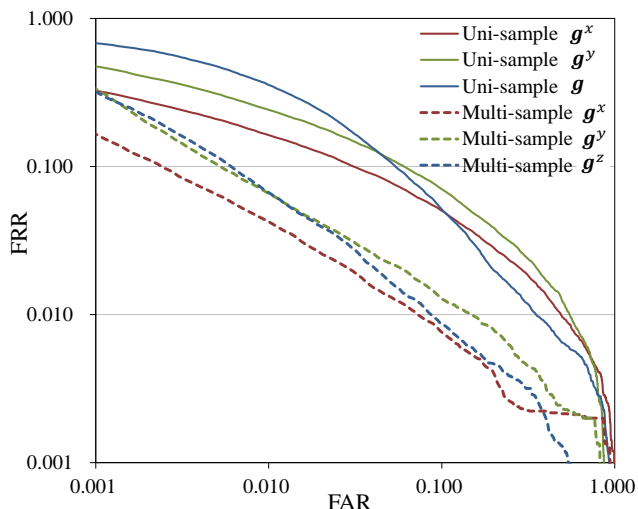


Figure 14: ROC curves of uni-sensor methods for three-axis angular velocity.

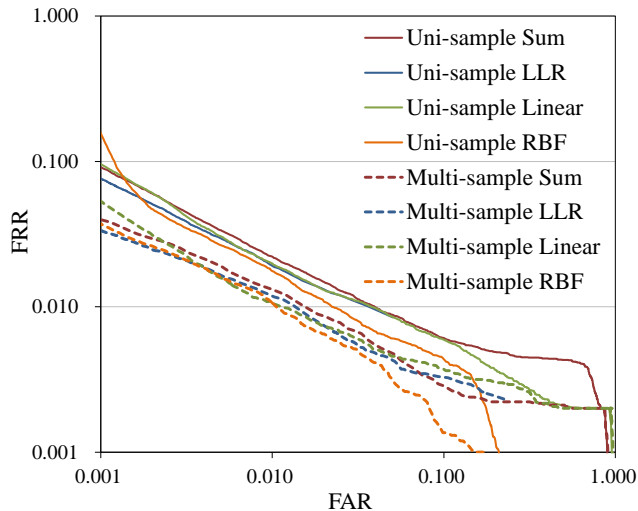


Figure 15: ROC curves of multi-sensor methods from four distances.

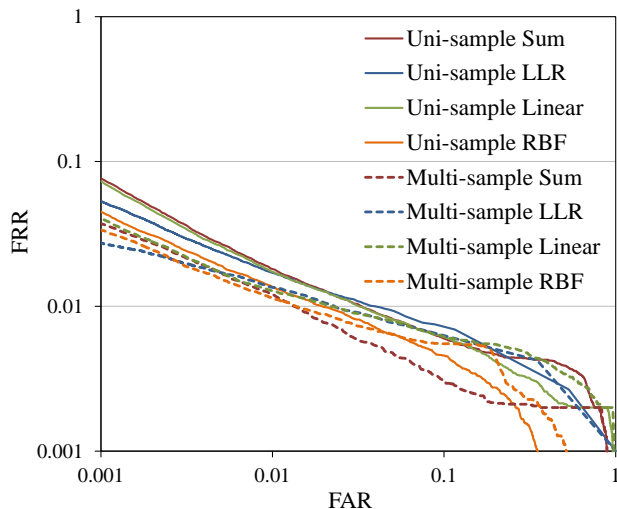


Figure 16: ROC curves of multi-sensor methods from seven distances.

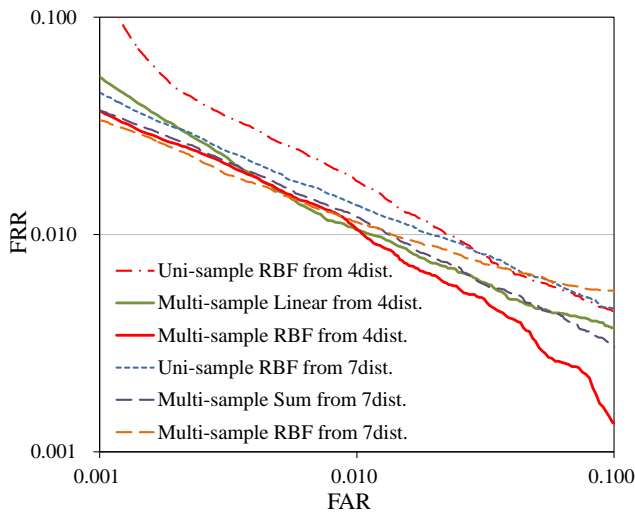


Figure 17: ROC curves of the best EER methods in each multi-sensor combination.

## 5 DISCUSSION

This research described here is an effort to improve the accuracy of gait-based authentication. We applied multi-sensor and multi-sample fusion to improve accuracy as compared with the uni-sensor and uni-sample method. The results of the tests are summarized in Tables 4, 5, and 6.

Comparing the effect of uni-sample and multi-sample, uni-sensor multi-sample (the best EER = 2.2%) is smaller than uni-sensor uni-sample (the best EER = 4.6%), giving a relative reduction in EER of 52.2%. Similarly, the multi-sensor multi-sample method from four distances (the best EER = 1.0%) is smaller than multi-sensor uni-sample method (the best EER = 1.4%), giving a relative reduction in EER of 28.6%. The multi-sensor multi-sample method from the seven distances (the best EER = 1.1%) is smaller than multi-sensor uni-sample method (the best EER = 1.2%), giving a relative reduction in EER of 8.3%. The results show that the multi-sample method is effective in gait-based authentication. However, in the case of multi-sensor authentication from the seven distances, the effect of multi-sample is smaller than the case of the other authentications.

Comparing the effect of multi-sensor, multi-sensor uni-sample from four distances is smaller than uni-sensor uni-sample, with a relative reduction of 69.9% in EER. EER of multi-sensor multi-sample from the four distances is smaller than EER of uni-sensor multi-sample, with a relative reduction in EER of 54.5%. Similarly, EER of multi-sensor uni-sample from seven distances is smaller than EER of uni-sensor uni-sample, with a relative reduction in EER of 73.9%. EER of multi-sensor multi-sample from seven distances is smaller than EER of uni-sensor multi-sample, with a relative reduction in EER of 45.5%. The results show that the multi-sensor method is effective in gait-based authentication.

Comparing the effect of fusion algorithms, SVM with RBF indicated the best performance in the four types of multi-sensor authentication. Hence, SVM with RBF is effective in gait-based authentication.

Comparing the effect of the multiple distances, in the uni-sample authentication, the best EER from seven distances show the smaller value than the best EER from four distances. However, the best EER of four distances show the smaller value than the best EER from seven distances in the multi-sample authentication. We think that Manhattan distances from three-axis acceleration signals ineffective for accuracy improvement in comparison with difference of direction of three-axis acceleration vectors. This is for the following reasons. EER from four distances shows almost same value of EER from seven distances. SVM with RBF and multi-sample from seven distances become significantly lower performance than SVM with RBF and multi-sample from four distances in the low FRR area.

Table 7 summarizes the best EERs of previous work with a uni-sensor. The conditions are different from those of our study, making simple comparison of the results of all the work difficult. However, we outperformed all of the previous methods. The work in [6] authenticated 50 subjects whose acceleration sensor was in a front trouser pocket. The condition of sensor location was similar to that of our experiment. The best result (EER = 7.3%) was obtained by calculating the Manhattan distance. The proposed method outperforms this previous work under the same sensor condition. Furthermore, our proposed method also outperforms the distance calculation and template generation methods of previous work on the same dataset.

In this experiment, to obtain the subjects' signals without effect of pocket form, the sensor unit was attached to their thigh. From the result of this experiment, we evaluated the accuracy based on the pure signals without noise caused by the pocket. However, when considering the case of actual use, we need to evaluate the accuracy of the proposed method under the condition of putting the sensors into subjects' pockets.

This study was researched based on the premise that walking patterns of all people were the feature which could identify only one person. This premise is not clear. However, the researches of gait recognition based on dynamic image achieved high accuracy with large number of the subjects. According to these researches, there is possibility that walking pattern is unique feature. Furthermore, it is not known whether the distribution of features from walking signals is uniform. It is important to clarify these issues for updating this research. To verify these things, we will need to collect the large scale dataset.

## 6 CONCLUSION

This paper proposed multi-sample and multi-sensor method for accuracy improvement of gait-based authentication and verified the effectiveness of the proposed methods.

First, we observed the relation among the steps and six-axis signals in order to extract the quasi-periodic signals generated by walking motion of the same gait phase order in all subjects by using two force sensors and a six-axis sensor. These findings show that it is possible to divide into quasi-periodic signals by extracting x-axis acceleration from local maxima to next local maxima.

Table 7: EERs of uni-sensor-based authentication work.

Reference	Number of subjects	Best EER[%]
Jani et al. [4]	36	7
Gafurov et al. [5]	22	16
Gafurov et al. [6]	21	5
Gafurov et al. [7]	50	7.3
Gracian et al. [8]	11	3
Derawi et al. [9]	60	5.7
This paper	50	1.0

Next, to improve the authentication accuracy, we proposed multi-sensor and multi-sample authentication methods. To find the appropriate methods for each process, we verified the authentication accuracy calculated by each method, distance calculation methods, fusion algorithms, multi-sensor, and multi-sample. From these experiments, we could find the appropriate methods to obtain the better authentication accuracy in the gait-based authentication.

We evaluated the proposed method with 50 subjects. The best EER performance was 1.0%, which was achieved by the combination of multi-sensor multi-sample using SVM with RBF from four distances. These results show that multi-sensor multi-sample authentication is useful for gait-based authentication. We confirmed that the proposed method using appropriate methods which were obtained from this study leads to better performance than the conventional methods.

In the future, we need to collect the gait data in an experimental condition that is similar to an actual use environment (e.g., a corner, a slope, with different type of pockets, and with different type of shoes) for the feasibility experiments. Furthermore, this experiment could indicate the combination effect of acceleration-based authentication to angular velocity-based authentication. However, it was not clear whether the combination of angular velocity-based authentication to acceleration-based authentication is effective. We think we will try to evaluate this question under the actual use environment, after collecting the large dataset.

## REFERENCES

[1] A.K. Jain, A. Ross, and S. Prabhakar, "An Introduction to Biometric Recognition," *IEEE Trans. Circuits and Systems for Video*, Vol.14, No.1, pp.4-20 (2004).  
 [2] F. Alonso-Fernandez, J. Fierrez, D. Ramos, and J. Ortega-Garcia, "Dealing with sensor interoperability in multi-biometrics: The UPM experience at the Biosecure multimodal Evaluation 2007," *Proc. of SPIE Defense and Security Symposium, Workshop on Biometric Technology for Human Identification*, pp.69440J-69440J (2008).  
 [3] X. Zhou and B. Bhanu, "Feature Fusion of Side Face and Gait for Video-based Human Identification," *Pattern Recognition*, Vol.41, pp.778-795 (2008).  
 [4] J. Mäntyjärvi, M. Lindholm, E. Vildjiounaite, S. Mäkelä, and H.A. Ailisto, "Identifying Users of Portable Devices from Gait Pattern with Accelerometers," *Proc. of*

*the IEEE International Conference on Acoustics, Speech and Signal Processing*, pp.973-976 (2005).  
 [5] D. Gafurov, E. Snekkenes, and T.E. Buvarp, "Robustness of Biometric Gait Authentication Against Impersonation Attack," *Proc. of the 1st International Workshop on Information Security (IS'06), OnTheMove Federated Conferences (OTM'06)*, Vol.4277, pp.479-488 (2006).  
 [6] D. Gafurov, K. Helkala, and T. Sondrol, "Biometric Gait Authentication Using Accelerometer Sensor," *Journal of Computers*, Vol.1, No.7, pp.51-59 (2006).  
 [7] D. Gafurov, E. Snekkenes, and P. Bours, "Gait Authentication and Identification using Wearable Accelerometer sensor," *Proc. of IEEE Workshop on Automatic Identification Advanced Technologies*, pp.220-225 (2007).  
 [8] G. Trivino, A. Alvarez-Alvarez, and G. Bailador, "Application of the Computational Theory of Perceptions to Human Gait Pattern Recognition," *Pattern Recognition*, Vol.43, pp.2572-2581 (2010).  
 [9] M.O. Derawi, P. Bours, and K. Holien, "Improved Cycle Detection for Accelerometer Based Gait Authentication," *Proc. of the 6th International Conference on Intelligent Information Hiding and Multimedia Signal Processing (IIH-MSP '10)*, pp.312-317 (2010).  
 [10] S. Mondal, A. Nandy, P. Chakraborty, and G.C. Nandi, "Gait Based Personal Identification System Using Rotation Sensor," *Journal of Emerging Trends in Computing and Information Sciences*, Vol.3, No.3, pp.395-402 (2012).  
 [11] A. Savitzky and M.J.E. Golay, "Smoothing and Differentiation of Data by Simplified Least-squares Procedures," *Anal. Chem.*, Vol.36, No.8, pp.1627-1639 (1964).  
 [12] F. Okumura, A. Kubota, Y. Hatori, K. Matsuo, M. Hashimoto, and A. Koike, "A Study on Biometric Authentication based on Arm Sweep Action with Acceleration Sensor," *Proc. of International Symposium on Intelligent Signal Processing and Communications, 2006(ISPACS '06)*, pp.219-222 (2006).  
 [13] S. BenYacoub, "Multi-Modal Data Fusion for Person Authentication using SVM," *Proc. 2nd Int. Conf. Audio-Video Based Biometric Person Authentication*, pp.25-30 (1999).  
 [14] N.V. Chawla, K.W. Bowyer, L.O. Hall, and W.P. Kegelmeyer, "SMOTE: Synthetic Minority Over-sampling Technique," *Journal of Artificial Intelligence Research*, Vol.16, pp.321-357 (2002).

(Received October, 11, 2015)



**Shinsuke Konno** received B.E. and M.S. from Hokkaido University in 2002 and 2004, respectively. He is currently a research associate at the National Institute of Technology, Hakodate College. His current research interests include mobile sensing and biometrics. He is a member of

IEICE, and IPSJ.



**Yoshitaka Nakamura** received B.E., M.S., and Ph.D. degrees from Osaka University in 2002, 2004 and 2007, respectively. He is currently a research associate at the School of Systems Information Science, Future University Hakodate. He is a member of IEEE, IEICE, and IPSJ.



**Yoh Shiraishi** received doctor's degree from Keio University in 2004. He is currently an associate professor at the Department of Media Architecture, School of Systems Information Science, Future University Hakodate, Japan. His research interests include database, mobile sensing

and ubiquitous computing. He is a member of IPSJ, IEICE, GISA and ACM.



**Osamu Takahashi** received master's degree from Hokkaido University in 1975. He is currently a professor at the Department of System Information Science at Future University Hakodate, Japan. His research interest includes ad-hoc network, network security, and

mobile computing. He is a member of IEEE, IEICE.